Journal of Power Sources 194 (2009) 558–567

Contents lists available at ScienceDirect

Journal of Power Sources

journal homepage: www.elsevier.com/locate/jpowsour

State of charge estimation in Ni–MH rechargeable batteries

R.H. Milocco[a,*], B.E. Castro[b]

[a] Grupo Control Automático y Sistemas (GCAyS), Depto. Electrotecnia, Facultad de Ingeniería, Universidad Nacional del Comahue, Buenos Aires 1400, 8300 Neuquén, Argentina
[b] Instituto de Investigaciones Fisicoquímicas Teóricas y Aplicadas (INIFTA), Universidad Nacional de La Plata, Suc 4, CC16 (1900), La Plata, Argentina

ARTICLE INFO

Article history:
Received 10 March 2009
Received in revised form 6 May 2009
Accepted 7 May 2009
Available online 18 May 2009

Keywords:
State of charge
Metal hydride battery
Wiener model
Least squared identification
Kalman filtering

ABSTRACT

In this work we estimate the state of charge (SOC) of Ni–MH rechargeable batteries using the Kalman filter based on a simplified electrochemical model. First, we derive the complete electrochemical model of the battery which includes diffusional processes and kinetic reactions in both Ni and MH electrodes. The full model is further reduced in a cascade of two parts, a linear time invariant dynamical sub-model followed by a static nonlinearity. Both parts are identified using the current and potential measured at the terminals of the battery with a simple 1-D minimization procedure. The inverse of the static nonlinearity together with a Kalman filter provide the SOC estimation as a linear estimation problem. Experimental results with commercial batteries are provided to illustrate the estimation procedure and to show the performance.

1. Introduction

The development of low-cost high capacity batteries is of great importance for large-scale production and application. Ni–MH batteries based on a hydrogen storage alloy have received and still receive much attention because of their higher energy density, superior charge–discharge characteristics and freedom from toxic materials. The state of charge (SOC) of a rechargeable battery is an important quantity as it is a measure of the amount of electrical energy available. In order to guarantee a good performance and lifetime of the battery, the SOC is usually kept within appropriate limits, for example $20\% \leq \text{SOC} \leq 90\%$, so the estimation of the SOC is essential for the battery to operate within these safe limits. Battery SOC estimation using available potential and current measured at the terminals of the battery is the goal of this paper.

There have been several approaches to estimate the state of charge of a battery. In [1] a review of impedance measurements to estimate SOC is presented. These approaches are based on the variation of the frequency response of the battery at different states of charge and other physical variables. In [2] an observer for linear time variant systems was used to estimate the open circuit voltage (OCV), which is related to the SOC, from an empirical battery model. Assuming observability of an extended model formulation, both parameters and state of charge are estimated at once. Plett [3] uses a simple dynamical model of one state, the SOC, which is in fact the integral of the current. An empirical relationship between SOC and measured current and potential is used together with the extended Kalman filter (EKF). Further improvements were obtained by adding new states related to the diffusional process inside the electrodes. In a different approach, Barbarissi et al. [4], presents the SOC estimation based on an electrochemical model taking into account the kinetics of the reactions and the diffusional process inside the electrode. The estimator used in this case consists of a simulation of the electrochemical model with the measured current/potential as inputs. SOC is estimated with the internal variables obtained by simulation.

In this work we estimate the SOC of Ni–MH rechargeable batteries based on an electrochemical model and using the Kalman filter. The main contributions of this paper are the following: First, the derivation of a complete model including both electrodes, Ni and MH, absorption/adsorption processes and double layer capacity. Second, the derivation of an electrochemical reduced order of the battery as a *Wienner model* formulation. It consists of two parts, a linear dynamic in cascade with a static nonlinearity. Third, we propose an identification procedure by using a simple 1-D optimization procedure. Fourth, the SOC estimation is performed in the framework of linear systems in which the estimation error bound, due to the presence of disturbances, can be optimized using a Kalman filter. The paper is organized as follows: In Section 2, the complete model of both electrodes is presented including kinetics of reactions, hydrogen diffusion process, and charge balances. Considering the fact that it will be used for SOC estimation, the simpler reduced order model is derived from the complete one. In Section 3, the functional relationship between SOC and hydrogen concentration is presented for different electrode geometries. In Section 4, the

* Corresponding author. Tel.: +54 299 4488305; fax: +54 299 4488305.
E-mail addresses: milocco@uncoma.edu.ar (R.H. Milocco), bcastro@inifta.unlp.edu.ar (B.E. Castro).

0378-7753/$ – see front matter © 2009 Elsevier B.V. All rights reserved.
doi:10.1016/j.jpowsour.2009.05.005

Nomenclature

a_n	effective transfer area of Ni interface
a_m	effective transfer area of MH interface
$E_n(t)$	potential at Ni–electrolyte interface
$E_m(t)$	potential at MH–electrolyte interface
E_{bat}	potential at the battery terminals
$E^{eq}_{n,ref}$	equilibrium potential of Ni interface at $x^{ref}_n(0,t) = 0.5$
$E^{eq}_{m,ref}$	Equilibrium potential of MH interface at $x^{ref}_m(0,t) = 0.5$
F	Faraday constant
h	sampling period
$I_{f_1}(t)$	Faradaic current of Ni electrode
$I_{f_2}(t)$	Faradaic current of MH electrode
I_{cn}	double layer capacitive current at Ni interface
I_{cm}	double layer capacitive current at MH interface
I_{bat}	current at the battery terminals
I^0_{1ref}	constant exchange current at Ni interface
I^0_{2ref}	constant exchange current at MH interface
$J_n(z,t)$	flux of hydrogen at position z of Ni electrode
$J_m(z,t)$	flux of hydrogen at position z of MH electrode
$J_n(z_i,t)$	flux of hydrogen at ith slice of Ni electrode
$J_m(z_i,t)$	flux of hydrogen at ith slice of MH electrode
$K_i(t)$	reaction rate
L	order of the Taylor expansion series
t	time
$x_n(z,t)$	H fractional concentration at position z of Ni electrode
$x_m(z,t)$	H fractional concentration at position z of MH electrode
$x_n(z_i,t)$	H fractional concentration at ith slice of Ni electrode
$x_m(z_i,t)$	H fractional concentration at ith slice of MH electrode
$x^n_0(t)$	short notation of $x_n(z_0,t)$
$x_i(t)$	ith state of simplified model
$\mathbf{x}(t)$	state vector of simplified model
$\mathbf{x}(kh)$	discrete-time state vector of simplified model
$\hat{\mathbf{x}}(kh)$	Estimated state vector using Kalman filter
$x_0(kh)$	discrete-time state $x_0(t)$
$x^{ref}_n(0,t)$	H reference fractional concentration at Ni interface
$x^{ref}_m(0,t)$	H reference fractional concentration at MH interface
$\mathbf{x}_n(t)$	vector of concentrations in Ni
$\mathbf{x}_m(t)$	vector of concentrations in MH
$\tilde{\mathbf{x}}(kh)$	estimation error vector
z	spatial position along axis z
z_i	discrete-spatial position of slice i along axis z
$\eta_n(t)$	incremental potential at Ni–electrolyte interface
$\eta_m(t)$	incremental potential at MH–electrolyte interface
$\theta(t)$	fractional surface concentration of MH_{ad}
θ_{ref}	surface concentration at the equilibrium reference state
θ_g	parameter vector of the static nonlinearity
θ_{gi}	parameter vector of the software sensor

simplified model is identified using a simple 1-D optimization procedure. The parameters of a proposed software sensor – to estimate the concentration at the surface of the Ni electrode to be used in SOC estimation – is also obtained in this section. In Section 5, a linear Kalman filtering strategy for the state estimation of hydrogen concentration is presented. Three experimental examples are used to illustrate the procedure and to show the performance of the proposed technique.

2. Model formulation

The nickel/metal hydride battery consists of a nickel positive electrode and a metal hydride negative electrode separated by a porous inert separator, being the whole assembly immersed in a highly concentrated, usually 30 percent of the weigh, KOH aqueous electrolyte. In Fig. 1 a scheme is shown. The main reactions during discharge are the reduction of nickel oxyhydroxide in the positive electrode and the oxidation of the metal hydride in the negative one, [5]. An adsorption/absorption reaction mechanism governs the insertion of hydrogen atoms in the metal [6,7]. The set of reactions are given as follows:

$$NiOOH + H_2O + e^- \overset{K_1,disch.}{\rightleftarrows} Ni(OH)_2 + OH^- \quad (1)$$

$$MH_{ad} + OH^- \overset{K_2,disch.}{\rightleftarrows} H_2O + M + e^- \quad (2)$$

$$M + SH_{ab} \overset{k^0_3,disch.}{\rightleftarrows} MH_{ad} + S, \quad (3)$$

being the reaction rates $K_i(t) = k^0_i exp(b\alpha_i E(t))$ for $i = 1, 2$ for electrochemical steps in (1) and (2) with constants k^0_i and $b = F/RT$, k^0_3 is the constant reaction rate due to the chemical reaction in (3), $E(t)$ the potential at the electrode interface, being $E_n(t)$ and $E_m(t)$ the potential at Ni and MH interfaces, respectively, and $\alpha_i \in [0, 1]$ are the symmetry factors. MH_{ad} is an adsorbed hydrogen atom at an active site on the alloy surface, and SH_{ab} is a hydrogen atom absorbed at an interstitial site in the alloy, located just beneath the surface, and S is an empty interstitial site. The process is reversed during charge with rate constants $K_{-i}(t) = k^0_{-i} exp(b(\alpha_i - 1)E(t))$ for $i = 1, 2$, and k^0_{-3} for reactions (1), (2), and (3), respectively. There are also secondary reactions due to oxygen evolution at the nickel electrode

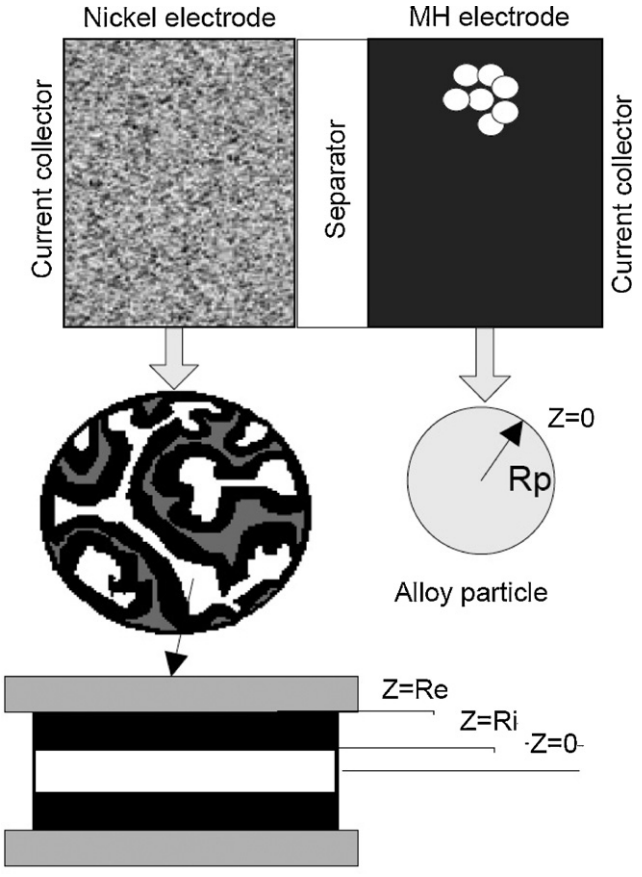

Fig. 1. Schematic diagram of the Ni/MH cell.

and oxygen reduction at the metal hydride electrode. However, in the operative SOC range of the battery (10–90%) the secondary reactions are insignificant compared with the main reaction. Since we are interested in modeling the dynamics in such range, the secondary reactions will be neglected in this work. Thus, the model considers the kinetics of the reactions taking place at the electrodes described by Eqs. (1)–(3). In order to complete the dynamics of the electrochemical processes involved, mass transport of H atoms in the metal hydride particles and Ni active material must be taken into account. Mass transport shall be modeled as a diffusional process and described in terms of Fick's laws. We will describe each process in detail.

Considering the global process of reaction (1) as the reaction of a "free hydrogen site", NiOOH, with H_2O to produce an "occupied hydrogen site", $Ni(OH)_2$ and OH^-, the faradaic current related to reaction (1) at the Ni electrode is governed by the following charge balance [8,9]:

$$I_{f_1}(t) = F\left(K_1(t)x_n(0,t) - K_{-1}(t)(1 - x_n(0,t))\right), \tag{4}$$

where $x_n(0,t) = c_n(0,t)/\bar{c}_n(0,t)$ is the fractional concentration of hydrogen atoms in the Ni active material at the electrochemical interface (Ni oxide/electrolyte interface, named spatial position $z = 0$ at time t). The hydrogen concentration, $c_n(z,t)$, and its maximum admissible value, $\bar{c}_n(z,t)$, define $x_n(z,t) = 1$ and $x_n(z,t) = 0$ for maximum and zero concentration at position z and time t, respectively. Let us introduce the incremental potential $\eta_n(t) = E_n(t) - E^{eq}_{n,ref}$ as the difference between the electrode potential and the equilibrium potential at the reference state $x^{\mathrm{ref}}_n(z_0,t) = 0.5$. Being the exchange current I^0_{1ref} defined by the expression

$$I^0_{1ref} = Fk^0_1 e^{b\alpha_1 E^{eq}_{n,ref}} = Fk^0_{-1} e^{b(\alpha_1-1)E^{eq}_{n,ref}}, \tag{5}$$

by replacing $\eta_n(t)$ in the expression of K_1 and K_{-1} in (4) and using (5) the current at the Ni electrode can be rewritten as

$$I_{f_1}(t) = I^0_{1ref}\left(e^{b\alpha_1\eta_n(t)}x_n(0,t) - e^{b(\alpha_1-1)\eta_n(t)}(1 - x_n(0,t))\right). \tag{6}$$

Using the same notation, the faradaic current balance at the MH electrode is given by reaction in (2) and can be written as

$$I_{f_2}(t) = -F\left(K_2(t)\theta(t) - K_{-2}(t)(1 - \theta(t))\right), \tag{7}$$

being $\theta(t)$ the fractional surface concentration of MH_{ad} species. As in the Ni–electrode, we define $\eta_m(t) = E_m(t) - E^{eq}_{m,ref}$ as the difference between the electrode potential and the equilibrium potential at the reference state $x^{\mathrm{ref}}_m(0,t) = 0.5$ (the fractional concentration of hydrogen atoms, SH_{ab}, at the metal hydride particles–electrolyte interface). Accordingly, the exchange current is given by

$$I^0_{2ref} = Fk^0_2 e^{b\alpha_2 E^{eq}_{m,ref}}\theta_{ref} = Fk^0_{-2} e^{b(\alpha_2-1)E^{eq}_{m,ref}}(1 - \theta_{ref}), \tag{8}$$

where θ_{ref} is the surface concentration at the equilibrium reference state. Taking into account the fast dynamical response of the hydrogen absorption reaction (HAR step given by reaction 3), equilibrium may be assumed and the following relationship is fulfilled [10]:

$$k^0_3(1 - \theta(t))x_m(0,t) = k^0_{-3}\theta(t)(1 - x_m(0,t)). \tag{9}$$

By replacing $\theta(t)$ from (9) in (7) and taking into account that $\theta_{ref} = 1/(K+1)$ with $K = k^0_{-3}/k^0_3$ – obtained with $x^{\mathrm{ref}}_m(0,t) = 0.5$ in (9)– and using (8), the expression of the faradaic current at the MH electrode can be written as

$$I_{f_2} = \frac{I^0_{2,ref}(K+1)}{x_m(z_0,t) + K(1 - x_m(z_0,t))}\left(x_m(0,t)e^{b\alpha_2\eta_m} - (1 - x_m(0,t))e^{b(\alpha_2-1)\eta_m}\right). \tag{10}$$

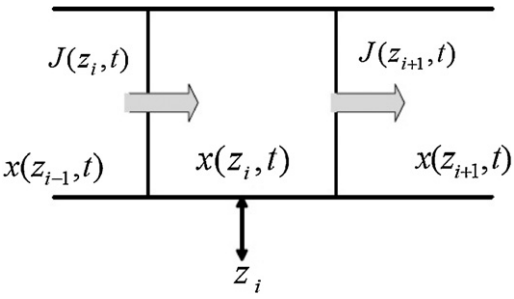

Fig. 2. Spatial discretization of the active film.

Considering the current during discharge to be positive, the complete current and potential balance is given by the series of both electrodes fulfilling

$$I_{bat} = -I_{f_1} - I_{cn} = I_{f_2} + I_{cm} \tag{11}$$

$$E_{bat} = E_n - E_m - I_{bat}R_i. \tag{12}$$

All the variables are function of time. I_{bat} and E_{bat} stand for the current and potential at the battery terminals; R_i is the resistance of the electrolyte; and I_{cn}, I_{cm} are capacitive currents due to the double layer at the Ni and MH electrode interface respectively, having the following expression:

$$I_{cn} = \frac{dE_n}{dt}C_{dl,n}; \quad I_{cm} = \frac{dE_m}{dt}C_{dl,m}; \tag{13}$$

where $C_{dl,n}$ and $C_{dl,m}$ are the double layer capacities of the electrode surfaces. The dynamics of hydrogen concentration in the electrodes are given by diffusional processes described by Fick's laws. The Ni electrode, represented schematically in Fig. 1, shall be described as a porous metallic structure, where the active material is deposited on the cylindrical pores of mean dimensions [5]. The active material on the pore walls forms a cylindrical film of average thickness, $d = R_e - R_i$, hydrogen diffusion taking place mainly in the radial direction. In a similar way, but considering spherical geometry particles, the hydrogen diffusion in metal hydride electrode is governed by Fick's laws. The analytical solution of Fick's laws is complex [11]. Then, in order to have a working expression of the diffusional processes, they can be approximated into a set of ordinary differential equations by using a spatial discretization. The spatial discretization is a very well-known method to approximate partial differential equations in ordinary differential equations. For details see [12,13], and also applied to *Ni–MH* batteries in [4]. Each diffusional process can be discretized along the space variable z by considering N slices of the metal with thickness Δz, as illustrated in Fig. 2. By denoting spatial position of ith slice as z_i, the dynamics of diffusional processes for both electrodes can be written as follows (see the Appendix A for a detailed derivation):

$$\frac{d\mathbf{x}_n(t)}{dt} = \mathbf{A}_n\mathbf{x}_n(t) + \mathbf{B}_n I_{f_1}(t) \tag{14}$$

$$x^n_0(t) = C_n\mathbf{x}_n(t) \tag{15}$$

where $x^n_0(t)$ is a short notation of $x_n(z_0,t)$, and

$$\mathbf{A}_n = \alpha\begin{bmatrix} -d_0 & d_0 & 0 & \cdots & 0 & 0 & 0 \\ 1 & -(1+d_1) & d_1 & \cdots & 0 & 0 & 0 \\ \vdots & \vdots & \vdots & \ddots & \vdots & \vdots & \vdots \\ 0 & 0 & 0 & \cdots & 1 & -(1+d_{N-1}) & d_{N-1} \\ 0 & 0 & 0 & \cdots & 0 & 1 & -1 \end{bmatrix},$$

$$\mathbf{C}_n = [1\,0\cdots 0], \quad \mathbf{B}_n = [\beta, 0, \cdots, 0]^T; \ \mathbf{x}_n(t) = [x_n(z_0,t), x_n(z_1,t), \ldots, x_n(z_N,t)]^T, \tag{16}$$

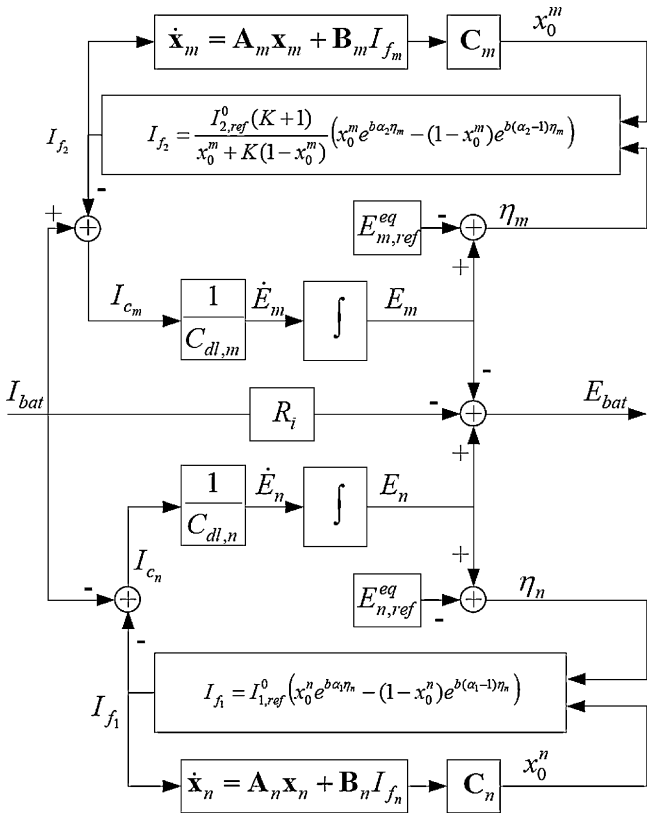

Fig. 3. Ni–MH battery model.

with $\alpha = D_n/\Delta z^2$, D_n is the diffusion coefficient, $\Delta z = \frac{R_e - R_i}{N+1}$, being R_e and R_i the exterior e interior radium in the cylindrical geometry, $\beta = 1/(Fa_n\bar{c}_n\Delta z)$ with a_n the effective transfer area, and $d_i = z_{i+1}/z_i = (2i+3)/(2i+1)$ for $1 \le i \le N$.

A similar approach can be followed for the metal electrode (see the Appendix A) by replacing $\Delta z = \frac{R_p}{N+1}$ with R_p the radium of the sphere, and $d_i = z_{i+1}^2/z_i^2 = (2i+3)^2/(2i+1)^2$ for $1 \le i \le N$.

Finally, the complete battery model is then given by Eqs. (6), (10)–(16). The equations of the diffusional process for the metal electrode, which are similar to (14)–(16), are also included in the complete battery model and depicted in Fig. 3.

2.1. Reduced complexity model

There are different reasons that justify the use of a simplified model to be used for SOC estimation. We present two important arguments: (i) In commercial Ni–MH batteries usually the negative electrode (MH electrode) has a higher effective capacity than the positive one (nickel oxyhydroxide/ nickel hydroxide electrode), being quite reasonable to assume that variations of the fractional hydrogen concentration in the metal hydride electrode may be neglected with respect to variations in the Ni electrode. Thus, the Ni electrode is sufficient to describe the dynamics of the energy storage in the battery. Consequently, the changes in E_{bat} are mainly due to changes in E_n, as reported in [5]. Accordingly, next, potential changes at the MH electrode shall be neglected, considering $E_m = E^{eq}_{m,ref}$. (ii) The maximum current is bounded for constructive reasons. Then, charge and discharge are mainly due to the low frequency components of the current, I_{bat}. Since the current passing throughout the double layer capacity contains mainly high frequency components, if I_{bat} is conveniently "low pass filtered", as described in Section 5.1, there are no significant differences in SOC estimation by neglecting the capacitive current I_{cn} and considering $I_{bat}(t) \simeq -I_{f1}(t)$ in (11). Then, in order to get a simplified model, we can use $I_{bat}(t) = -I_{f1}(t)$ in Eq. (6) as input and potential $E_{bat} = E^{eq}_{n,ref} - E^{eq}_{m,ref} + \eta_n(t) - I_{bat}R_i$ as output. However, to use this approach it is necessary for $\eta_n(t)$ in (6) to be a function of x_0 and I_{bat}. In other words, there should be a unique value of $\eta_n(t)$ for each couple of values (x_0^n, I_{bat}). In order to show that this requirement is fulfilled, let us start by noting that in (6) the concentration x_0^n is a function of the couple (η_n, I_{bat}), as follows:

$$x_0^n = \frac{-I_{bat} + I^0_{1ref}e^{b(\alpha_1-1)\eta_n}}{e^{b(\alpha_1-1)\eta_n} + e^{b\alpha_1\eta_n}} = f(\eta_n, I_{bat}). \tag{17}$$

A continuous function f is one to one (and hence invertible) if and only if it is either strictly increasing or decreasing with not local maxima or minima. In our case the derivative with respect to η_n after some algebraical manipulation can be written as

$$\frac{\partial x_0^n}{\partial \eta_n} = \frac{b(\alpha_1-1)e^{b\alpha_1\eta_n}(1-x_0^n) - x_0^n\alpha_1 be^{\alpha_1 b\eta_n}}{e^{b\alpha_1\eta_n} + e^{b(\alpha_1-1)\eta_n}}. \tag{18}$$

Taking into account that $x_0^n \in (0,1)$, and $\alpha_1 \in (0,1)$, the derivative above is always negative. Thus, the inverse function $\eta_n = f^{-1}(x_0, I_{bat})$ exists, hence there is only one value of η_n for each couple (x_0^n, I_{bat}).

Taking into account these considerations, the complete model depicted in Fig. 3 can be simplified as shown in Fig. 4. We will show it later that experimental results are accurately represented by the proposed model.

Remark 1. The simplified model is a cascade of a linear time invariant dynamical system and a static nonlinearity. Such kind of model is called *Wiener model*. A Wiener model consists of a linear dynamic system followed by a static nonlinearity. The input and output are measured, but not the intermediate signal. Then, the identification of both parts as black boxes are difficult to obtain [14]. Using the electrochemical model we propose a successful approach in the next section.

Before to proceeding with the identification of the model parameters, we show in next section that the gain β in (16) can be known directly from the structure of the diffusion model. Also we show how it is related to a working expression to compute the SOC.

3. The state of charge

The SOC in the battery is determined by integrating the current as follows:

$$\mathrm{SOC}(t) = \frac{1}{Q_{max}}\left(Q_0 + \int_0^t I_{bat}(\tau)d\tau\right), \tag{19}$$

where Q_0, and Q_{max} are the initial and maximum electrode charge. The quantity Q_{max} is called *capacity* of the battery and it is defined as the product of the constant current and the time required to reach the maximum charge, starting with battery completely discharged, $Q_0 = 0$. Thus, SOC is the unity for battery completely charged and zero for completely discharged. We derive the expression for SOC in the nickel electrode by integrating, with respect to time, both

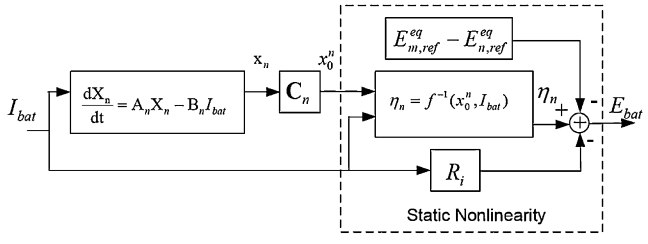

Fig. 4. Simplified battery model.

sides of equation (14) in which we consider $I_{bat}(t) = -I_{f1}(t)$. Since in the simplified model only the Ni electrode will be considered, the subindex of the fractional concentration will be dropped for clarity as follows: $x_n(z_i, t)$ will be denoted as $x_i(t)$, and vector $\mathbf{x}_n(t)$ as $\mathbf{x}(t)$. After integrating and using (19), we have

$$\mathbf{x}(t) - \mathbf{x}(0) = \int_0^t A\mathbf{x}(\tau)d\tau - \mathbf{B}Q_{max}(\mathrm{SOC}(t) - \mathrm{SOC}(0)). \tag{20}$$

Using the elements of matrix A defined in (16), the previous is equivalent to the following set of equations:

$$\begin{aligned}
x_0(t) &= \alpha d_0 \int_0^t (x_1(\tau) - x_0(\tau))d\tau - \beta Q_{max}(\mathrm{SOC}(t) - \mathrm{SOC}(0)) + x_0(0)\\
x_1(t) &= \alpha \int_0^t (x_0(\tau) - x_1(\tau)) + d_1(x_2(\tau) - x_1(\tau))d\tau + x_1(0)\\
&\vdots = \vdots\\
x_{N-1}(t) &= \alpha \int_0^t (x_{N-2}(\tau) - x_{N-1}(\tau)) + d_{N-1}(x_N(\tau) - x_{N-1}(\tau))d\tau + x_{N-1}(0)\\
x_N(t) &= \alpha \int_0^t (x_{N-1}(\tau) - x_N(\tau))d\tau.
\end{aligned} \tag{21}$$

By replacing the integral term of $x_N(t)$ from the last equality in the expression of $x_{N-1}(t)$ we have

$$x_{N-1}(t) = \alpha \int_0^t (x_{N-2}(\tau) - x_{N-1}(\tau))d\tau - d_{N-1}x_N(t) + x_{N-1}(0).$$

By following the procedure from bottom to top on the set of equations (21), the following equality is obtained:

$$\mathrm{SOC}(t) = cnt - \frac{x_0(t) + d_0x_1(t) + d_0d_1x_2(t) + \cdots + d_0\cdots d_{N-1}x_N(t)}{\beta Q_{max}}, \tag{22}$$

where the constant cnt is given by

$$cnt = \frac{x_0(0) + d_0x_1(0) + d_0d_1x_2(0) + \cdots + d_0\cdots d_{N-1}x_N(0)}{\beta Q_{max}} + \mathrm{SOC}(0) \tag{23}$$

Considering the stationary case, zero current in the limit when time goes to infinity, the concentrations $x_i(\infty)$ for $0 \le i \le N$ are equal. For battery completely charged all the concentrations are equal to zero which corresponds to SOC equal to the unity and vice versa. Then, from (22) a set of two equations with two unknowns, cnt and β, can be formed. The solution gives $cnt = 1$ and

$$\beta = \frac{1 + d_0 + d_0d_1 + \cdots + d_0\cdots d_{N-1}}{Q_{max}} \tag{24}$$

Finally, the expression for $\mathrm{SOC}(t)$ is given by

$$\mathrm{SOC}(t) = 1 - \frac{x_0(t) + d_0x_1(t) + d_0d_1x_2(t) + \cdots + d_0\cdots d_{N-1}x_N(t)}{\beta Q_{max}} \tag{25}$$

with β given by (24).

Remark 2. Considering different steady states, ($I_{bat} = 0$) at the equilibrium ($t \to \infty$), the charge balance (6) gives the relationship between OCV and SOC, often used to compute the SOC, as follows:

$$x_0(\infty)e^{b\alpha_1\eta_n} = (1 - x_0(\infty))\, e^{b(\alpha_1 - 1)\eta_n} \tag{26}$$

which – using the fact that $\mathrm{SOC} = 1 - x_0(\infty)$ – leads to the fulfillment of the following SOC/OCV relationship:

$$\begin{aligned}
\eta &= E_{bat} - E^{eq}_{m,ref} + E^{eq}_{n,ref} = \frac{1}{b}\log\left(\frac{1 - x_0(\infty)}{x_0(\infty)}\right)\\
&= \frac{1}{b}\log\left(\frac{\mathrm{SOC}(\infty)}{1 - \mathrm{SOC}(\infty)}\right) \quad = f^{-1}(x_0, 0)
\end{aligned} \tag{27}$$

In the next section we identify the parameters of the model to be used for SOC estimation.

4. Model parameter identification

The model parameters that remain to be identified are α in (16) and the parameters corresponding to the static nonlinearity. The static nonlinearity is a soft function that can be well approximated by using different approaches. We choose to approximate the function with a Taylor series expansion of multivariable functions, which can be written as a linear regression problem as follows:

$$E_{bat} = -E^{eq}_{m,ref} + E^{eq}_{n,ref} - I_{bat}R_i + f^{-1}(x_0, I_{bat}) = g(x_0, I_{bat}) = \varphi_g\theta_g, \tag{28}$$

where θ_g is a column vector of parameters and φ_g, a row vector of signals as follows:

$$\varphi_g = [1,\ I_{bat},\ x_0,\ I_{bat}x_0,\ I^2_{bat},\ x_0I_{bat},\ x^2_0,\ \text{higher orders}];$$

$$\theta_g = \begin{pmatrix} \theta_1 \\ \vdots \\ \theta_L \end{pmatrix}, \tag{29}$$

where L depends on the series order approximation of the static nonlinearity. In expression (29) the ith element of θ_g is the derivative of ith order of the unknown function $g(x_0, I_{bat})$ evaluated at a given coordinates. We choose to expand around the stationary coordinates $(x_0, I_{bat}) = (0, 0)$. Using this representation, we propose the following procedure to estimate α and θ_g: (i) Discharge completely and recharge with a known small amplitude current during a given time. After a long resting time, the known stationary values $\mathbf{x}(0)$ are reached. (ii) Excite the battery with a time varying current and obtain a record of M sampled of both $I_{bat}(kh)$, and $E_{bat}(kh)$. (iii) Choose an arbitrary value of the scalar α within a given griding interval. (iv) Using this value of α in Eq. (14), obtain the zero-hold discrete-time system as follows:

$$\mathbf{x}((k+1)h) = \mathbf{A}_d\mathbf{x}(kh) - \mathbf{B}_dI_{bat}(kh) \tag{30}$$

$$x_0(kh) = C_d\mathbf{x}(kh), \tag{31}$$

where h is the sampling period, and (A_d, B_d, C_d) is the zero-hold discrete-time system obtained from (A_n, B_n, C_n) as follows [15]:

$$A_d = e^{A_nh}; \quad B_d = \int_0^h e^{As}B_n ds; \quad C_d = C_n; \tag{32}$$

and $\mathbf{x}(kh)$ is the sampled vector of concentrations at times $t = kh$. (v) Using the discrete-time model, the M samples of $I_{bat}(kh)$, and $E_{bat}(kh)$, and the known initial concentrations, obtain the estimated sequence $x_0(kh)$ by simulation using (30) and (31). (vi) Using the M values of $I_{bat}(kh)$, $E_{bat}(kh)$, and $x_0(kh)$ obtained in the previous step, the value of parameters θ_g are fitted by using the least squared approximation as follows:

$$\theta_g = (\Phi^T\Phi)^{-1}\Phi^TY, \tag{33}$$

where

$$\Phi = [\varphi_g(1)^T, \ \ldots, \ \varphi_g(k)^T, \ \ldots, \ \varphi_g(M)^T,]^T \tag{34}$$

$$\varphi_g(k) = [1, \quad I_{bat}(kh), \quad x_0(kh), \quad I_{bat}(kh)x_0(kh),$$
$$I_{bat}^2(kh), \quad x_0(kh)I_{bat}(kh), \quad x_0^2(kh), \quad \text{higher order elements}] \tag{35}$$

$$Y = [E_{bat}(h), \ \ldots; E_{bat}(kh), \ \ldots; E_{bat}(Mh)]^T. \tag{36}$$

(vii) Compute the sum of the least squared error of the estimation as

$$\sum_{i=1}^{M} e_i^2 = (Y - \Phi\theta_g)^T(Y - \Phi\theta_g). \tag{37}$$

Save the result, choose a new value of α and return to step (iii). The procedure continues for all the griding values of α in the considered interval. Finally, we adopt the coupled α and θ_g which gives the lowest least squared error subjected to the constraints that the simulated concentration $x_0(kh)$ lies in the interval [0, 1].

Remark 3.

- It is important to note that the computational complexity is 1-D which is solved by performing steps (iii)–(vii) repeatedly for different values of α within the grid interval of one dimension. It must also be noted that the reduced complexity is due to the fact that we have used an analytical model description of the battery.
- The surface concentration sampled sequence, $x_0(kh)$, is obtained by simulation and it is unique and different for different values of α. The interval of possible values of α can be known from the analytical expression $\alpha = D_n(N+1)^2/(R_e - R_i)^2$ where typical values of D_n are in the interval (10^{-9} to 10^{-10}), N is given by the number of slices of the spatial discretization, and $(R_e - R_i)$ depends on the battery.
- The identifiability is governed by the minimum least squared problem (33) which states that the estimated vector θ_g converges to the true value if the input I_{bat} is *persistently excited* (PE), which means the current variations need to be rich enough to satisfactory identify the parameters θ_g, [16,17].
- Since the function $x_0 = f(\eta, I_{bat})$ has inverse $\eta_n = f^{-1}(x_0, I_{bat})$, then, from (28) the function $E_{bat} = g(x_0, I_{bat})$ has also inverse given by $x_0 = g^{-1}(E_{bat}, I_{bat})$. Then, the value of parameters that minimizes the Euclidean norm of the cost in (37) also minimizes the Euclidean norm of the differences between the real and estimated concentration $x_0(kh)$.
- Since we are interested in low frequencies, a previous low pass (LPF) filtering of sequences $I_{bat}(kh)$ and $E_{bat}(kh)$ must be done. Some guidelines about how to choose the cut frequency of the LPF will be given in the next section.

It is useful, for further use in SOC estimation, to have a practical way to estimate the value of $x_0(kh)$ from measurements $E_{bat}(kh)$ and $I_{bat}(kh)$. To this end, we need to identify the inverse function $x_0 = g^{-1}(E_{bat}, I_{bat})$ which works in fact as a software sensor of concentration $x_0(kh)$. It can be done by using the estimated sequence $x_0(kh)$, obtained in the optimization procedure described before, and finding the coefficients of the linear regression model of the inverse function $x_0(kh) = g^{-1}(E_{bat}(kh), I_{bat}(kh)) \approx \varphi_{gi}(kh)\theta_{gi} = x_0^m(kh)$. The estimated parameters θ_{gi}, in the sense of minimum least squared, can be obtained in a similar procedure as the one explained above but replacing Φ and Y in (33), by

$$\Phi = [\varphi_{gi}(1)^T, \ \ldots, \ \varphi_{gi}(k)^T, \ \ldots, \ \varphi_{gi}(M)^T,]^T \tag{38}$$

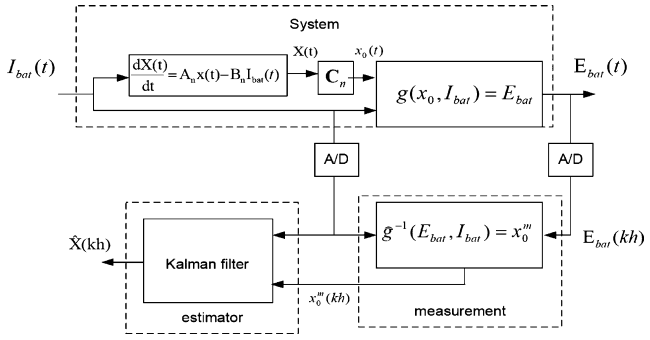

Fig. 5. SOC estimation.

$$\varphi_{gi}(k) = [1, \ I_{bat}(kh), \ E_{bat}(kh), \ I_{bat}(kh)E_{bat}(kh), \ I_{bat}^2(kh),$$
$$E_{bat}(kh)I_{bat}(kh), \ E_{bat}^2(kh), \ \text{higher order elements}] \tag{39}$$

$$Y = [x_0(h), \ \ldots, x_0(kh), \ \ldots, x_0(Mh) \ ]^T. \tag{40}$$

Note that the estimated value $x_0^m(kh) = \varphi_{gi}(kh)\theta_{gi}$, obtained from the measured current $I_{bat}(kh)$ and potential $E_{bat}(kh)$, is an approximation of the true value $x_0(kh)$. It will be used, in next section, as a software sensor of fractional concentration at the interface.

5. SOC estimation and results

The basic idea to estimate the SOC is to use the expression (25) together with (24) employing estimated values of the vector concentrations $\mathbf{x}(kh)$ that will be named $\hat{\mathbf{x}}(kh)$. To this end, let us have first the estimated value of $x_0^m(kh)$ as it was explained in the last section. It is interpreted as the true value, $x_0(kh)$, corrupted by measurement zero mean random noise, errors due to the imperfect interpolation, and possible unmodeled dynamics. Using this measure the concentration vector $\mathbf{x}(kh)$ is estimated by means of the Kalman filter. The equation of the Kalman filter are given by

$$\hat{\mathbf{x}}((k+1)h) = A_d\hat{\mathbf{x}}(kh) + B_d I_{bat}(kh) + K_k(x_0^m(kh) - C_d\hat{\mathbf{x}}(kh)) \tag{41}$$

$$K_k = A_d P_k C_d (R_2 + C_d P_k C_d^T)^{-1} \tag{42}$$

$$P_{k+1} = A_d P_k A_d^T + R_1 - A_d P_k C_d^T (R_2 + C_d P_k C_d^T)^{-1} C_d P_k A_d^T \tag{43}$$

where P_k, R_1, and R_2 are the positive definite covariance matrices of errors in the estimations, noise disturbances at the concentrations, and measurement noise, respectively. Notice that the global convergence is guaranteed since the diffusional process is linear. Moreover, in the ideal case where the disturbances at the states and measurement noise can be modeled as gaussian white noise with zero mean, the error covariance matrix between real and estimated vector concentrations is given by $\mathcal{E}(\mathbf{x}(kh) - \hat{\mathbf{x}}(kh))(\mathbf{x}(kh) - \hat{\mathbf{x}}(kh))^T = P_k$ in (43) where $\mathcal{E}$ means expected value. No more details about Kalman filter will be given since there is a wide reference to this respect. See for example [15,3]. The complete scheme is depicted in Fig. 5.

The measure $x_0^m(kh)$, provided by the software sensor and based on data interpolation, is an approximation of the true state $x_0(kh)$. This error affects the estimation of the vector $\hat{\mathbf{x}}(kh)$ in (41). In order to analyze how the estimation is affected by this error, let us assume that the measure $x_0^m(kh)$ consists of the sum of the true value, given by $x_0(kh) = C_d\mathbf{x}(kh)$, plus a difference given by $\Delta_{\mathbf{x}}(kh)$, which is in fact the error introduced by the interpolation procedure. Then, the error between the real and estimated concentrations can be obtained by substracting (41) from (30) as follows:

$$\tilde{\mathbf{x}}(kh + h) = \mathbf{x}(kh + h) - \hat{\mathbf{x}}(kh + h) \tag{44}$$

$$= (A_d - K_k C_d)\tilde{\mathbf{x}}(kh) + K_k\Delta_{\mathbf{x}}(kh) \tag{45}$$

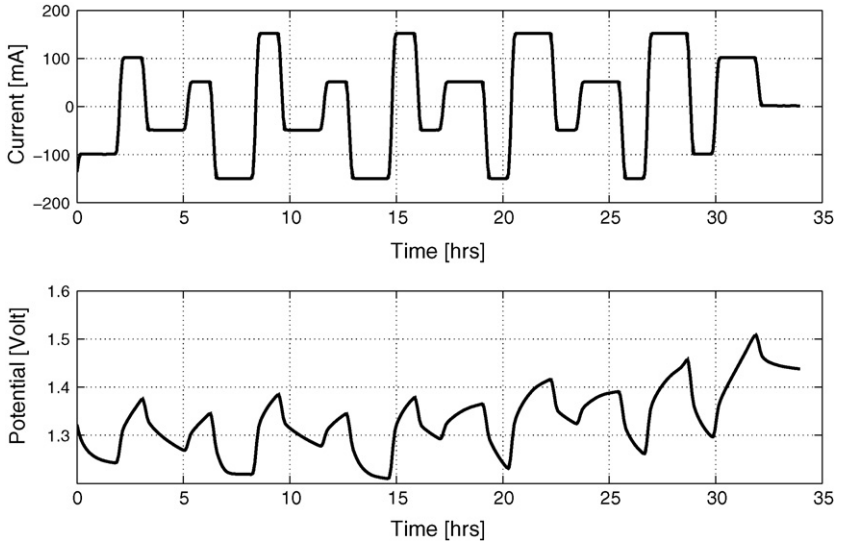

Fig. 6. True and low pass filtered current and potential for experiment 1.

By denoting $F = A_d - K_k C_d$, the solution of the above difference equation is given by

$$\tilde{\mathbf{x}}(kh) = F^k \tilde{\mathbf{x}}(0) + \sum_{j=0}^{k-1} F^{k-j-1} K_k \Delta_{\mathbf{x}} \tag{46}$$

It consists of two terms, the first is the transient due to the error at the initial conditions $\tilde{\mathbf{x}}(0)$, and the second one is due to the uncertainties in the software sensor $\Delta_{\mathbf{x}}$. The transient is governed by the eigenvalues of matrix F which are tuned by the gain Kalman matrix K_k in a way that short transient need large values of K_k. The second term is a discrete-time convolution between the transient and the product of the gain matrix K_k by the interpolation error $\Delta_{\mathbf{x}}(kh)$. Then, large values of the gain matrix K_k produces short transient but increases the effect of measurement errors. Conversely, a low filter gain produces a long transition but mitigates the effect of the uncertainties. Using the covariance matrix of the measurement error $R_2 = \mathcal{E}(\Delta_{\mathbf{x}} \Delta_{\mathbf{x}}^T)$, the gain of the Kalman filter solve optimally the tradeoff between both terms in (46) and it depends inversely on R_2 according with Eq. (42). In the next section we will use this analysis to interpret the experimental results.

5.1. Experimental results

The examples presented in this paper are based on measurements made in rechargeable batteries Duracell AAA/HR03/DX2400, NiMH/1,2/800 mAh. The used experimental setup consists in a power unit driven by a personal computer throughout an I/O card with A/D and D/A conversions in a MATLAB environment. Three different experiments exciting the battery with a variant current load (charge and discharge) using a sampling time of $h = 8$ s are presented. The first two experiments are used to identify the model parameters (α, θ_g) together with the software sensor parameters θ_{gi}. Both experiments are also used to estimate SOC. In the third experiment, the SOC is estimated using the values of the model parameters identified with the first two experiments.

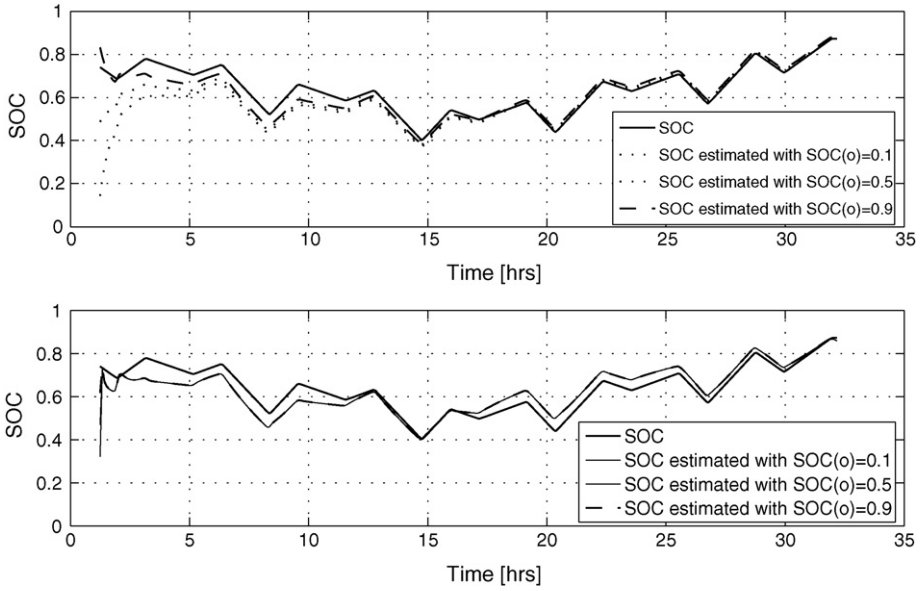

Fig. 7. SOC estimation for experiment 1. Upper, with $R_2 = 10$. Lower, with $R_2 = 0.1$.

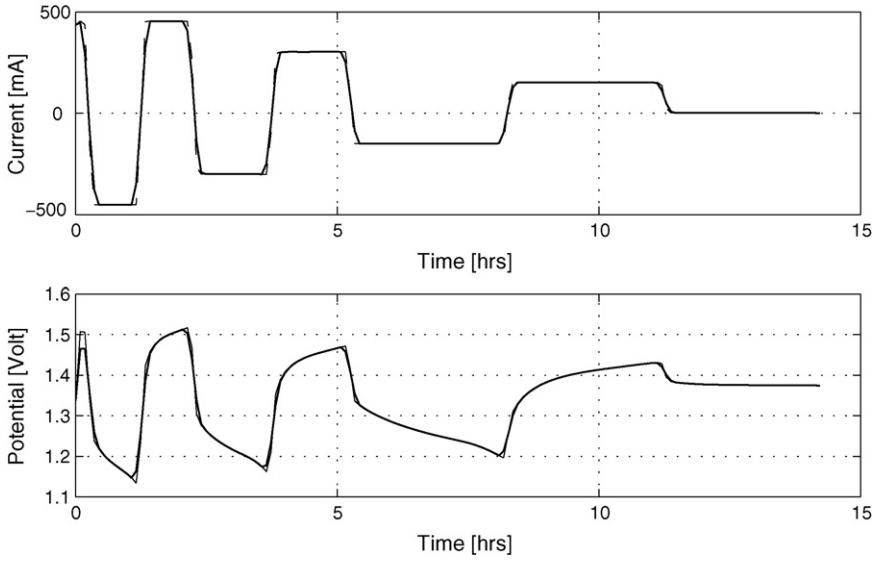

Fig. 8. True and low pass filtered current and potential for experiment 2.

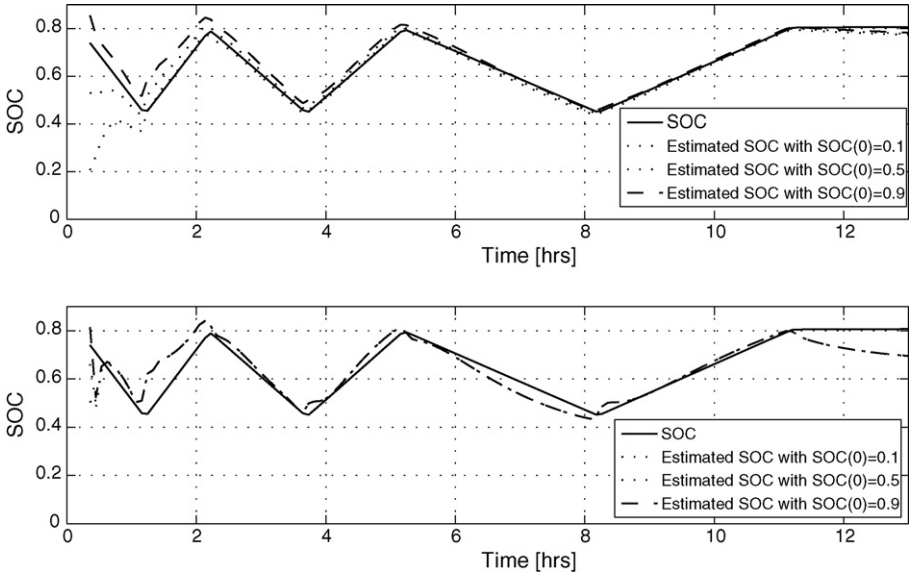

Fig. 9. SOC estimation for experiment 2. Upper, with $R_2 = 10$. Lower, with $R_2 = 0.1$.

Before each experiment the battery was discharged completely and recharged with a small amplitude known current. After a long resting time, the stationary values $\mathbf{x}(0)$ were perfectly known. Then, by integrating the current we also knew the real SOC. For each experiment current (I_{bat}) and potential (E_{bat}) at the terminal of the battery were recorded. In order to estimate the SOC, first both current and potential samples were low pass pre-filtered in order to eliminate the high frequency components. The filter used is a zero phase shift filter with the following structure:

$$s^f(kh) = \frac{1}{201}\sum_{i=-100}^{100} s(kh), \tag{47}$$

where $s(kh)$ is the sampled signal and $s^f(kh)$ is the filtered signal. This filtering task can be done on line, at the same time that the samples are obtained and considering, in our case, the necessary delay of 100 samples due to the noncausality of the filter. The criterion for choosing the cutoff frequency of the LPF depends on the battery. Using the recorded files of current and potential, in the identification stage, we started with a low cutoff frequency and iteratively it was increased until the error between the estimated and real SOC reached some admissible bound.

After filtering the signals were re-sampled at period $T = 5.33$ min. The current and potentials together with their filtered version for the three experiments are shown in Figs. 6, 8, and 10. Using a partition number $N = 30$, the first and second experiments were used to identify parameter α. By taking a value of $R_e - R_i = 10^{-3}$ cm, the search interval of the 1-D optimization procedure was [0.1, 1] giving $\alpha = 0.397$ and its corresponding θ_g and θ_{gi}. The value of β for the chosen model structure is 2.0855×10^{-4} coulomb.

With the identified values, SOC estimations were performed using the first and second experiments. In all the experiments the initial concentration values of the Kalman filter are arbitrarily fixed in 0.1, 0.5, and 0.9. There were used two different values of matrix covariance of the measurement error, $R_2 = 10$, and $R_2 = 0.1$, for computation of Kalman gain matrix K_k. Large value of R_2 gives small filter gain with relatively long transient and relatively good match to the true SOC. Opposite, small value of R_2

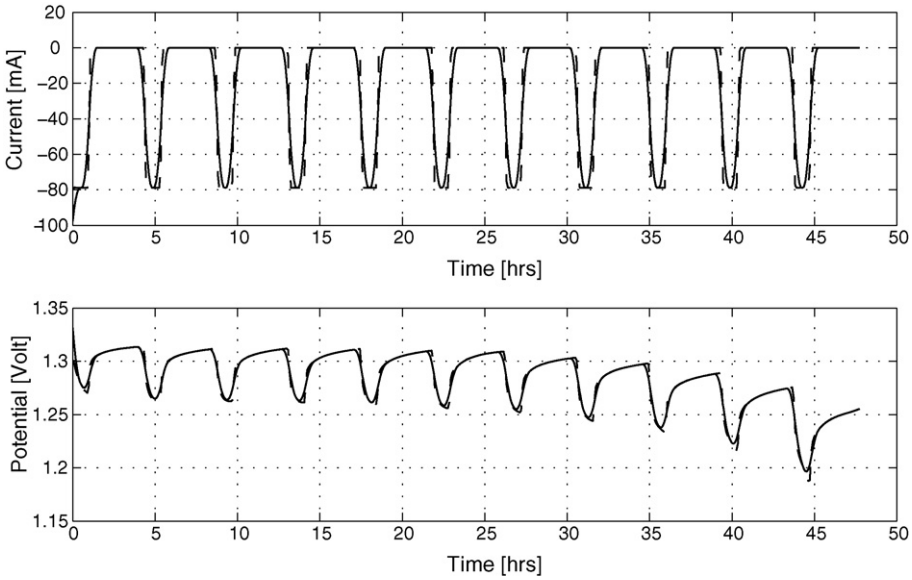

Fig. 10. True and low pass filtered current and potential for experiment 3.

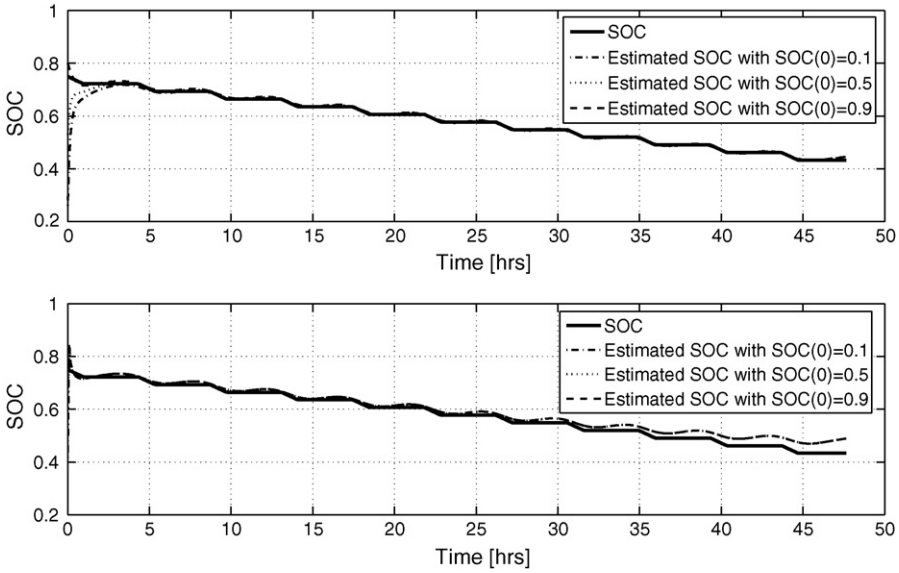

Fig. 11. SOC estimation for experiment 3. Upper, with $R_2 = 10$. Lower, with $R_2 = 0.1$.

gives high gain value with short transient but with a poor fit of the real SOC, due to the amplification of the measurement error. In Figs. 7 and 9 the estimated SOC, using both gain values, are depicted for first and second experiments. The optimal gain value can be obtained by knowing the value of R_2. It can be obtained from the interpolation procedure in the identification stage. It must be noted that as the interpolation error is smaller, the better the estimates.

The study of different interpolation methods than the linear regression used in this work, like splines [19], kernel [18], or Kriging [20] between others, to obtain software sensors with minimum error will be grounds for future research.

With the model parameters and smoothing filter properly selected in the identification stage, the SOC in third experiment is performed and depicted in Fig 11. Also two different gain matrix, $R_2 = 10$, and $R_2 = 0.1$, was employed in order to show the effect on the estimates. It must be noted that a good fitting of software sensor parameter is a crucial point to improve the results.

6. Conclusions

A complete electrochemical model of two electrodes of Ni–MH rechargeable batteries for SOC estimation was presented. Taking into account constructive reasons, the two-electrode model has been reduced to a simpler one-electrode model which belongs to the family of the Wiener models. The simplified model takes into account only the slow current variations, which are in fact the components that change the SOC. Using the kinetic equations, the two parts of the Wiener model, the dynamic linear and the static nonlinearity were identified by using 1-D optimization method to tune the parameters. The interval search is bounded by previous knowledge of typical parameter values.

The proposed method allows the estimation of the state of charge in Ni–MH rechargeable batteries using a simplified electrochemical based model by means of a software sensor and a Kalman filter to estimate the concentration inside the Ni electrode. Using this setup, minimum covariances of the estimation errors between

real and estimated concentrations due to external disturbances are obtained. Also the bound of the estimation errors are known. The expression of SOC as a function of the estimated concentrations for different electrode particles geometry was given. The method was used in experiments with commercial batteries reaching the expected performance.

Acknowledgements

This work was supported by the Consejo Nacional de Investigaciones Científicas y Técnicas (CONICET), Agencia Nacional de Promoción Científica y Técnica, Universidad Nacional del Comahue and Universidad Nacional de La Plata; all of República Argentina.

Appendix A.

The diffusion process in the Ni electrode is described by the cylindrical form of Fick's laws considering only the radial direction (coordinate z) as follows:

$$J_n(z,t) = -D_n \bar{c}_n \frac{\partial x_n(z,t)}{\partial z} \tag{48}$$

$$\frac{\partial x_n(z,t)}{\partial t} = D_n \left(\frac{\partial^2 x_n(z,t)}{\partial z^2} + \frac{1}{z} \frac{\partial x_n(z,t)}{\partial z} \right) \tag{49}$$

$$\frac{\partial x_n(z,t)}{\partial t} = -\frac{1}{\bar{c}_n} \frac{\partial [z J_n(z,t)]}{z \partial z}, \tag{50}$$

where $J_n(z,t)$ is the flux of hydrogen diffusing from the surface to the interior of the electrode at spatial position z and time t, and $J_n(z_0,t) = I_{f_1}/(Fa_n)$. If each cell is small enough, the concentration $x(z_i,t)$ in the $i-th$ cell $(0 \le i \le N)$, (see Figure(2)), can be considered constant with input and output hydrogen flow given by $J(z_i,t)$ and $J(z_{i+1},t)$ respectively. Using this spatial discretization together with the forward and backward approximation of the derivative, Eqs. (48)–(50) can be written as follows:

$$J_n(z_i,t) = -\frac{D_n \bar{c}_n}{\Delta z} (x(z_i,t) - x(z_{i-1},t)) \tag{51}$$

$$\frac{dx(z_i,t)}{dt} = -\frac{1}{\bar{c}_n z_i \Delta z} (z_{i+1} J_n(z_{i+1},t) - z_i J_n(z_i,t)), \tag{52}$$

Using these relationships and considering a boundary condition for the flux $J(z_N,t) = 0$ at the active material/metallic substrate interface ($z = R_e$), the diffusional process can be described by the set of Eqs. (14)–(16).

In a similar way, but considering the spherical geometry of the metal hydride particles, the equations governing the H concentration profile in the MH electrode are given by:

$$J_m(z,t) = -D_m \bar{c}_m \frac{\partial x_m(z,t)}{\partial z} \tag{53}$$

$$\frac{\partial x_m(z,t)}{\partial t} = -\frac{1}{\bar{c}_m z^2} \frac{\partial \left[z^2 J_m(z,t) \right]}{\partial z}, \tag{54}$$

where $J_m(z,t) D_m$ is the diffusion coefficient and $J_m(z_0,t) = I_{f_2}/(Fa_m)$ being a_m the effective transfer area. A similar discrete-spatial state model is derived for the metal electrode by just replacing $\Delta z = \frac{R_p}{N+1}$ with R_p the radium of the sphere, and $d_i = z_{i+1}^2/z_i^2 = (2i+3)^2/(2i+1)^2$ for $1 \le i \le N$.

References

[1] F. Huet, Journal of Power Sources 70 (1998) 59–69.
[2] J. Chiasson, B. Vairamohan, IEEE Transactions on Control Systems Technology 13 (3) (2005) 465–470.
[3] G. Plett, Journal of Power Sources 134 (2004) 252–261, 262–276, 277–292.
[4] O. Barbarisi, R. Canaletti, L. Glielmo, M. Gosso, F. Vasca, Proceedings of the IEEE Conference on Decision and Control, Las Vegas, Nevada, USA, 2002, pp. 1739–1744.
[5] B. Paxton, J. Newman, Journal of the Electrochemical Society 144 (11) (1997) 3818–3831.
[6] Ch. Wang, Journal of the Electrochemical Society 145 (6) (1998) 1801–1812.
[7] E.B. Castro, R.H. Milocco, Journal of Electroanalytical Chemistry 579/1 (2005) 113–123.
[8] Z. Mao, et al., Journal of the Electrochemical Society 141 (1994) 54.
[9] P. de Vidts, R. White, Journal of the Electrochemical Society 142 (1995) 1509.
[10] A. Visintin, E.B. Castro, S.G. Real, W.E. Triaca, C. Wang, M.P. Soriaga, Electrochimica Acta 51 (2006) 3658–3667.
[11] J. Crank, The Mathematics of Diffusion, Oxford Univ. Press, New York, 1975.
[12] D. Britz, Digital Simulation in Electrochemistry, 2nd Edition, Springer-Verlag, 1988.
[13] A. Lasia, D. Gregoire, Journal of the Electrochemical Society 142 (10) (1995) 3393–3399.
[14] Tokunbo. Ogunfunmi, Adaptive Nonlinear System Identification, Springer Science, 2007.
[15] K.J. Åström, Introduction to Stochastic Control Theory, Prentice Hall, 1970.
[16] T. Soderstrom, T. Stoica, System Identication, Prentice-Hall, Englewood Cliffs, NJ, 1989.
[17] L. Ljung, System Identification Theory for the User, Prentice-Hall, Englewood Cliffs, NJ, 1987.
[18] D.W. Scott, S.J. Sheather, Communications in Statistics: Theory and Methods 14 (1985) 1353–1359.
[19] H. Prautzsch, W. Bohem, M. Paluzny, Bezier and B-Spline Techniques, Springer Verlag, 2002.
[20] Milocco R. Gatti, A. Giaveno, Hydrometallurgy 71 (October (1–2)) (2003) 89–96.